2009

Anomalous H I In Ngc 2997

Kelley M. Hess

D. J. Pisano

Eric M. Wilcots

Jayaram N. Chengalur

The Astrophysical Journal, 699:76–88, 2009 July 1 doi:10.1088/0004-637X/699/1/76

ANOMALOUS H I IN NGC 2997

Kelley M. Hess[1], D. J. Pisano[2,3], Eric M. Wilcots[1], and Jayaram N. Chengalur[4]
[1] Department of Astronomy, University of Wisconsin-Madison, Madison, WI 53706, USA; hess@astro.wisc.edu, ewilcots@astro.wisc.edu
[2] Department of Physics, West Virginia University, P.O. Box 6515, Morgantown, WV 26506-6315, USA; dpisano@nrao.edu
[3] NRAO, P.O. Box 2, Green Bank, WV 24944, USA
[4] NCRA (TIFR) Pune 411007, India; chengalur@ncra.tifr.res.in
Received 2008 December 19; accepted 2009 April 23; published 2009 June 9

ABSTRACT

We present deep H I observations of the moderately inclined spiral galaxy, NGC 2997. The goal of these observations was to search for H I clouds in the vicinity of NGC 2997 analogous to the high-velocity clouds of the Milky Way and gain insight into their origins. We find evidence for the presence of a galactic fountain as well as the accretion of intragalactic material, however we do not identify any large clouds of H I far from the disk of the galaxy. NGC 2997 has a thick, lagging H I disk that is modeled with a vertical velocity gradient of 18–31 km s^{-1} kpc^{-1}. Anomalous velocity H I clouds with masses of order 10^7 $M_\odot$, which cannot be explained by galactic fountain models allow us to estimate a lower limit to the accretion of extragalactic gas of 1.2 $M_\odot$ yr^{-1}. The number and mass of these clouds have implications for cosmological simulations of large-scale structure and the presence of dark matter halos. We have used values from the literature to estimate a star formation rate of 5 ± 1 $M_\odot$ yr^{-1} and to derive a new distance to NGC 2997 of 12.2 ± 0.9 Mpc using published Tully–Fisher relations.

Key words: galaxies: individual (NGC 2297) – galaxies: ISM – galaxies: kinematics and dynamics – galaxies: structure

1. INTRODUCTION

In the Milky Way Galaxy, 21 cm observations of neutral atomic hydrogen (H I) provide a unique probe of the structure and dynamics of the interstellar medium. Muller et al. (1963) and others have identified clumps of H I emission with motions that are inconsistent with Galactic rotation. Formally, these high-velocity clouds (HVCs) are identified by either having a line-of-sight velocity, $|v_{LSR}|$, greater than 90 km s^{-1} with respect to the local standard of rest or else differ from the rotational velocity of the disk by greater than 50 km s^{-1} at a given Galactic longitude (Wakker & van Woerden 1997). Despite over 40 years of study, the origin of these HVCs remains a mystery. Our position within the Milky Way's disk provides a unique perspective of their spatial distribution. However, because the clouds do not obey Galactic rotation, distance measurements rely on the serendipitous position of stars and stellar spectroscopy to find distance brackets (e.g., Thom et al. 2006, 2007; Wakker et al. 2007, 2008) or other coincidences, such as the association of the Magellanic Stream with the Magellanic Clouds, or the interaction of Smith's Cloud (Lockman et al. 2008) and the Magellanic Stream (McClure-Griffiths et al. 2008) with the Galactic disk. Other HVCs may be tidal debris (e.g., Lockman 2003; Putman et al. 2004). Such coincidences yield distances to individual HVCs of order 10 kpc, but are quite rare and tell us little about the population as a whole. Accurate distances to H I clouds allow us to calculate their masses and to map their positions about the Galaxy and thereby differentiate between several HVC formation scenarios, which in turn have implications for cosmology and structure formation, chemical enrichment, and halo dynamics.

To explain the pervasive structure of Galactic HVCs across the sky, one must invoke multiple explanations. The Magellanic Stream is likely the result of tidal interactions with the Large and Small Magellanic Clouds. For other HVCs, Shapiro & Field (1976) and Bregman (1980) postulated that a galactic fountain mechanism could be responsible for raising hot gas into the Galactic halo where it would cool, condense, and then rain back down on the disk. Meanwhile, Oort (1970) proposed that these H I clouds are primordial leftovers that are just now being accreted by the Milky Way. This theory was revived recently by Blitz et al. (1999) and Braun & Burton (1999) who suggested that some types of HVCs were associated with low-mass dark matter halos seen in models of ΛCDM galaxy formation (Klypin et al. 1999). HVCs may also be produced by a cooling, condensing hot halo (e.g., Maller & Bullock 2004; Fukugita & Peebles 2006; Sommer-Larsen 2006; Peek et al. 2008). These theories have different predictions for the mass distribution, the vertical distance from the disk, and the metallicity for the clouds (see Wakker & van Woerden 1997, and references therein). But in either case, their presence would not be unique to our own Galaxy: in order to gain insight into the Galactic HVC population we observe other nearby spiral galaxies.

As the closest large spiral galaxy to the Milky Way, M 31 is an excellent test bed in which to search for HVC analogs. Thilker et al. (2004) found ∼20 discrete objects within 50 kpc of the M 31 disk that range in H I mass between 10^5 and 10^7 $M_\odot$ and can be characterized by a steep power law distribution. The authors suggest that these clouds may trace the dark matter halos around M 31 that are predicted from ΛCDM models. However, many of the clouds show velocity continuity implying that they may be tidal remnants associated with the stellar stream of M 31, or part of the H I bridge between M 31 and M 33 (Westmeier et al. 2005).

Observing edge-on galaxies reveals the vertical distribution of gas. The first, and subsequently, the most well studied galaxy for extraplanar H I is the edge-on spiral NGC 891 (e.g., Swaters et al. 1997). The deepest published observations probe to H I masses of 9.3×10^4 $M_\odot$ and a column density of 1.6×10^{18} cm^{-2} (Oosterloo et al. 2007). These observations show that NGC 891 has a large H I halo that extends vertically out to 14 kpc from the thin H I disk and, in one quadrant, out to 22 kpc, contributing nearly 30% of the total H I mass of the galaxy. This halo is characterized by differential rotation, but it lags behind the rotation of the disk by 15 km s^{-1} kpc^{-1}. Studies of

NGC 891 and other nearly edge-on galaxies imply that there is a significant link between the amount of star formation in the disk (as measured by Hα or radio continuum), and the properties of the lagging halo, which is believed to be evidence for gas circulation by a galactic fountain (Swaters et al. 1997; Heald et al. 2006a, 2006b, 2007). In general, they find that the scale height and the velocity gradient decrease with increasing star formation rate. Unfortunately, observations of edge-on galaxies are unable to tell us about either the position of clouds around the disk, or their vertical motion—the latter of which plays a part in identifying HVCs in the Milky Way.

In face-on galaxies H I at anomalous velocities and H I holes may be the result of gas accretion (e.g., M 101; van der Hulst & Sancisi 1988) or massive star formation (e.g., NGC 628; Kamphuis & Briggs 1992). The mass and morphology of clouds are frequently used to discriminate between high-velocity complexes that are likely to be infalling extragalactic gas versus galactic fountain gas energized by supernovae (SNe). In the case of accretion, the gas tends to be located in the outer portions of the galaxy and is more massive. In the star formation case, the gas clouds tend to have lower masses and are associated with regions of Hα or UV emission, or H I holes (e.g., Boomsma et al. 2009). The largest H I holes in M 101 may be the result of recent collisions with extragalactic clouds; SNe are ruled out because of the energy requirement to account for the amount of H I removed from the disk, and there is no evidence from UV or radio continuum data to support extraordinary star formation activity (van der Hulst & Sancisi 1988). NGC 6946 has an H I plume and large-scale asymmetries probably related to tidal encounters (Kamphuis & Sancisi 1993; Boomsma et al. 2009), as well as high-velocity gas and holes related to star formation. From the mass in the high-velocity gas, Kamphuis & Sancisi (1993) estimate an SN rate of 1 per 100 years to feed a galactic fountain, which is roughly consistent with the six SNe that have been observed in the galaxy this century.

Inclined galaxies have the benefits of both edge-on and face-on observations. One can distinguish the presence of extraplanar H I gas that lags behind the rotation of the disk and identify anomalous velocity gas with some sense of its location with respect to the disk while, at the same time, look for sites of active star formation that would be obscured in edge-on galaxies. There are a number of good examples of this. Position–velocity (hereafter PV) slices of NGC 2403 show H I gas above and below the thin disk rotating 25–50 km s^{-1} slower (Schaap et al. 2000; Fraternali et al. 2002), analogous to the extraplanar gas in NGC 891. Furthermore, channel maps show counter-rotating gas (Fraternali et al. 2001, 2002). In other examples, an asymmetry in the distribution of diffuse gas in NGC 253 is evidence for merger or accretion activity (Boomsma et al. 2005). Meanwhile Hα emission, from star formation activity, is correlated with high-velocity gas in NGC 6822 (de Blok & Walter 2006). H I holes have been observed in NGC 4559 that are attributed to SN explosions or stellar winds (Barbieri et al. 2005).

In order to better understand the origin of HVCs in the Milky Way and those seen around M 31, it is essential to observe a number of galaxies with similar properties that are well situated for detailed study. NGC 2997 is the largest spiral galaxy in the loose galaxy group, LGG 180 (Garcia 1993). This galaxy group was one of six observed by Pisano et al. (2007) in a Parkes survey of nearby Local Group analogs to search for intra-group HVC candidates. No HVC analogs were found in any of the groups down to a mass limit $\lesssim 10^7\ M_\odot$. We chose NGC 2997 for deep, high-resolution observations because of its similarities to the Milky Way and M 31 in mass, luminosity, and star formation rate. It is a relatively isolated galaxy (no known companions within 110 kpc), it is moderately inclined with respect to the line of sight ($\sim 33^\circ$), and it has with a well behaved rotation curve. NGC 2997 was also chosen because it cannot be confused with Galactic or Local Group H I emission. Given a healthy star formation rate, it would not be surprising to find evidence for a lagging H I disk; its inclination allows us to investigate the position and kinematics of clouds with respect to the galactic disk in simple rotation. With these observations we identify extraplanar H I and HVC analogs associated with galactic fountains, galaxy formation, and tidal debris and use the characteristics of such HVCs to discriminate between their possible origins.

The observations of NGC 2997 and data reduction are described in Section 2. The resulting data are described in Section 3 including the results from modeling each H I component in NGC 2997. In Section 4, we consider possible origins of the extraplanar gas of the thick disk and the anomalous velocity H I clouds, and compare the H I in NGC 2997 to that of other galaxies. We also derive the star formation rate and distance of NGC 2997, and discuss how it affects the constraints on the origins of HVCs. We conclude in Section 5.

2. OBSERVATIONS & DATA REDUCTION

In 2006 January, we observed NGC 2997 with the Australia Telescope Compact Array (ATCA) for 28 hr in the EW352 configuration. These observations were in addition to archival ATCA data (from project C453) for NGC 2997 taken during 1995 and 1996, amounting to a total of 59 hr in six different configurations (Table 1). The data were flagged and calibrated using the standard procedures in Miriad (Sault & Kileen 2008). From 2007 January 15–26, we observed the galaxy for a total of 61 hr in 7–8 hr blocks with the Giant Metrewave Radio Telescope (GMRT). The GMRT is comprised of 30 antennas in a fixed "Y"-configuration with 14 antennas within 1 km and a maximum baseline of 25 km. The data were flagged and calibrated in AIPS at the GMRT using the standard procedures. Each night was individually imaged and inspected before being combined to create our final data cube. All observations were taken at a velocity resolution of 6.596 km s^{-1}.

To combine the data, the reduced GMRT observations were written out of AIPS and read into Miriad.[4] The visibility data were combined in Miriad with the task UVAVER, and cleaned using the task MOSSDI. We imaged 120 channels centered on the galaxy using a robustness of 2 and down-weighted the longest baselines from the GMRT. We derive a distance to NGC 2997 of 12.2 Mpc using published Two Micron All Sky Survey (2MASS) Tully–Fisher relations (hereafter TF; Masters et al. 2008) that we adopt throughout the paper. Discussion of this derivation is left to Section 4.3 in order to not take away from the focus of this paper on the H I properties of the galaxy. At this distance, our observations have a spatial resolution of $14'' = 0.8$ kpc. Altogether, our final cube has a rms noise of $\sigma = 0.404$ mJy km s^{-1} beam^{-1} channel^{-1}. At 5σ we achieve a mass sensitivity of $4.7 \times 10^5\ M_\odot$ channel^{-1} and a column density of 9.6×10^{19} cm^{-2} beam^{-1} channel^{-1}.

[5] In Miriad, the imported image headers were incomplete: we had to set the rest frequency to 1.420405752 GHz and, for the purposes of estimating the rms noise before imaging, we added the correct values for the system temperature (76 K) and system gain (0.22 Jy K^{-1} antenna^{-1} $\times$ 30 antennas), http://www.gmrt.ncra.tifr.res.in/gmrt_hpage/Users/doc/spec_mod.pdf.

Table 1
Summary of ATCA Observations

Date	Configuration/ Max Baseline (m)[a]	Observing Time (hr)
1995 Oct 27	1.5D/1439 (4439)	10
1995 Nov 7	6A/2923 (5939)	14
1995 Dec 15	6C/2786 (6000)	13
1996 Jan 21	750C/750 (5020)	12
1996 Jan 23	750B/765 (4500)	11
1996 Feb 22	1.5C/1485 (4500)	9
2006 Jan 7	EW352/352 (4439)	8.5
2006 Jan 8	EW352/352 (4439)	8.5
2006 Jan 9	EW352/352 (4439)	11

Note.
[a] Maximum separation between antennas, excluding (and including) the 6 km antenna.

3. RESULTS

We present our data cube in the form of channel maps in Figures 1–3. These channel maps have been clipped at the 3σ level to emphasize the galactic emission. The figures illustrate the general rotation of NGC 2997, but also show evidence of a thick disk and additional H I that is moving at velocities inconsistent with a rotating thin disk.

In Figure 4, we present moment maps created from the data cubes: the optical Digitized Sky Survey (DSS) image with H I contours, the total H I intensity map, the velocity field, and the velocity dispersion (moments 0–2). The moments are calculated independently for each pixel within a specified clip range—in our case, it is calculated from pixels containing emission above 5σ of our rms sensitivity in order to avoid large outliers, particularly on the outskirts of the galaxy where the noise is increasing with distance from the pointing center. In the optical image, it becomes evident that the H I gas is extended to the northwest with respect to the optical disk. However, the intensity weighted velocity map looks fairly well behaved; there is no direct evidence that the galaxy has been disturbed by a strong encounter. Finally, the velocity dispersion map shows that the greatest dispersion occurs in the center likely due to beam smearing effects and due to intense star formation as suggested by strong radio continuum emission at the center of the galaxy.

Figure 5 shows the integrated H I profile over the area of the entire galaxy. Summing the emission in this profile yields a total flux for NGC 2997 of 226.6 Jy km s^{-1}. This compares to 162.3 Jy km s^{-1} from HIPASS (Meyer et al. 2004). However, the latter value is likely to be low since the HIPASS measurement assumed the galaxy was unresolved. At a distance of 12.2 Mpc, our measured flux corresponds to a total H I mass of $7.96 \times 10^9\ M_\odot$.

We are interested in understanding the nature of the H I in NGC 2997 and identifying gas clouds that are analogous to the HVCs observed in the Milky Way. In decomposing the galaxy, we find there are three components that contribute to its total H I content. A thin disk dominates the total H I emission and can be modeled by a Gaussian profile with a velocity dispersion of 11 ± 3 km s^{-1}. We modeled and fitted a rotation curve to this thin disk, however, there is additional gas that appears as a wing on the side of the thin disk's velocity profile toward the systemic velocity. This "thick disk" contributes approximately 16%–17% of the total H I mass and has a velocity dispersion of $\sim$16 km s^{-1}. While this second component shows regular rotation, it lags behind the thin disk at a relatively constant rate. The third component consists of H I emission that cannot be explained in terms of either disk component, and some of which is counter-rotating. These three components stand out in Figure 6.

Table 2
Properties of NGC 2997

Property	Value
Hubble Type	SAc[a]
Optical Center (J2000)	$09^h45^m38\overset{s}{.}8\ -31^\circ11'27\overset{''}{.}9$[a]
Optical Extent	$8\overset{'}{.}9 \times 6\overset{'}{.}8$[a]
Distance	12.2 Mpc[b]
Radio Center (J2000)	$09^h45^m35\overset{s}{.}9\ -31^\circ11'27\overset{''}{.}8$
Radio Extent	$15\overset{'}{.}6 \times 11\overset{'}{.}1$[c]
Systemic Velocity	1089 ± 5 km s^{-1}
Inclination, i	$32\overset{\circ}{.}3 \pm 0\overset{\circ}{.}3$
Position Angle	$107\overset{\circ}{.}1 \pm 0\overset{\circ}{.}6$
Integrated Flux Density	226.6 Jy km s^{-1}
H I Mass, $M_{\rm H\,I}$	$7.96 \times 10^9\ M_\odot$[b]
Maximum $v_{\rm rot}$	226 ± 2 km s^{-1}
Dynamical Mass, $M_{\rm dyn}$	$2.1 \times 10^{11}\ M_\odot$
Velocity gradient, $\frac{dv}{dz}$	18–31 km s^{-1} kpc^{-1}
Scale Height, z	0.7 ± 0.2 kpc
Cylindrical Height, $z_{\rm cyl}$	0.5 ± 0.1 kpc
Star Formation Rate	$5 \pm 1\ M_\odot$ yr^{-1}

Notes. Unless otherwise stated, the values in Table 2 are derived from this work.
[a] Optical position and extent obtained from the NASA/IPAC Extragalactic Database.
[b] Distance and H I mass are derived from the 2MASS TF relations of Masters et al. (2008).
[c] Measured from 3σ contours along major and minor axes.

Table 2 summarizes the properties we derive for the galaxy. We calculate a new distance to NGC 2997 based on the 2MASS TF relations from Masters et al. (2008). The radio center, systemic velocity, inclination, position angle, and the maximum rotational velocity come from our rotation curve fit to the velocity field. The integrated flux and $M_{\rm H\,I}$ come directly from the data cube. $M_{\rm dyn}$ is calculated from the maximum rotational velocity. The velocity gradient, scale height, and cylindrical height come from our best-fit model of the extraplanar H I. The star formation rate is estimated from values in the literature. Sections 3.1–3.3 and Section 4 (Discussion) describe in detail how we arrive at these values.

3.1. Modeling the Thin Disk

As illustrated by Figure 6, the H I profile toward most positions in NGC 2997 is dominated by a narrow velocity component with a dispersion of 11 ± 3 km s^{-1}. To model it, we clipped the data cube at 10% of the galaxy's peak emission (in a manner similar to Fraternali et al. 2002) and fit a Gaussian to this upper part of the velocity profiles. By clipping the emission at this level we prevent the subsequent analysis of NGC 2997's thin disk from being biased by broad, low column density H I velocity components. We fit a rotation curve to the thin disk following the procedure of Begeman (1989). We assume that the position angle and inclination of the galaxy are constant for all radii (we assume an ideal, flat disk), and from this we derive a systemic velocity of 1089 ± 5 km s^{-1}, a position angle of $107\overset{\circ}{.}1 \pm 0\overset{\circ}{.}6$ and an inclination of $32\overset{\circ}{.}3 \pm 0\overset{\circ}{.}3$. The errors are the average errors found for rings between 5–30 kpc, however, Figure 7 shows that there is a gradient in the position angle, which has not been taken into account.

The top panel of Figure 7 shows our best-fit rotation curve. It rises out to $\sim$12 kpc, then slowly declines to greater than 25 kpc.

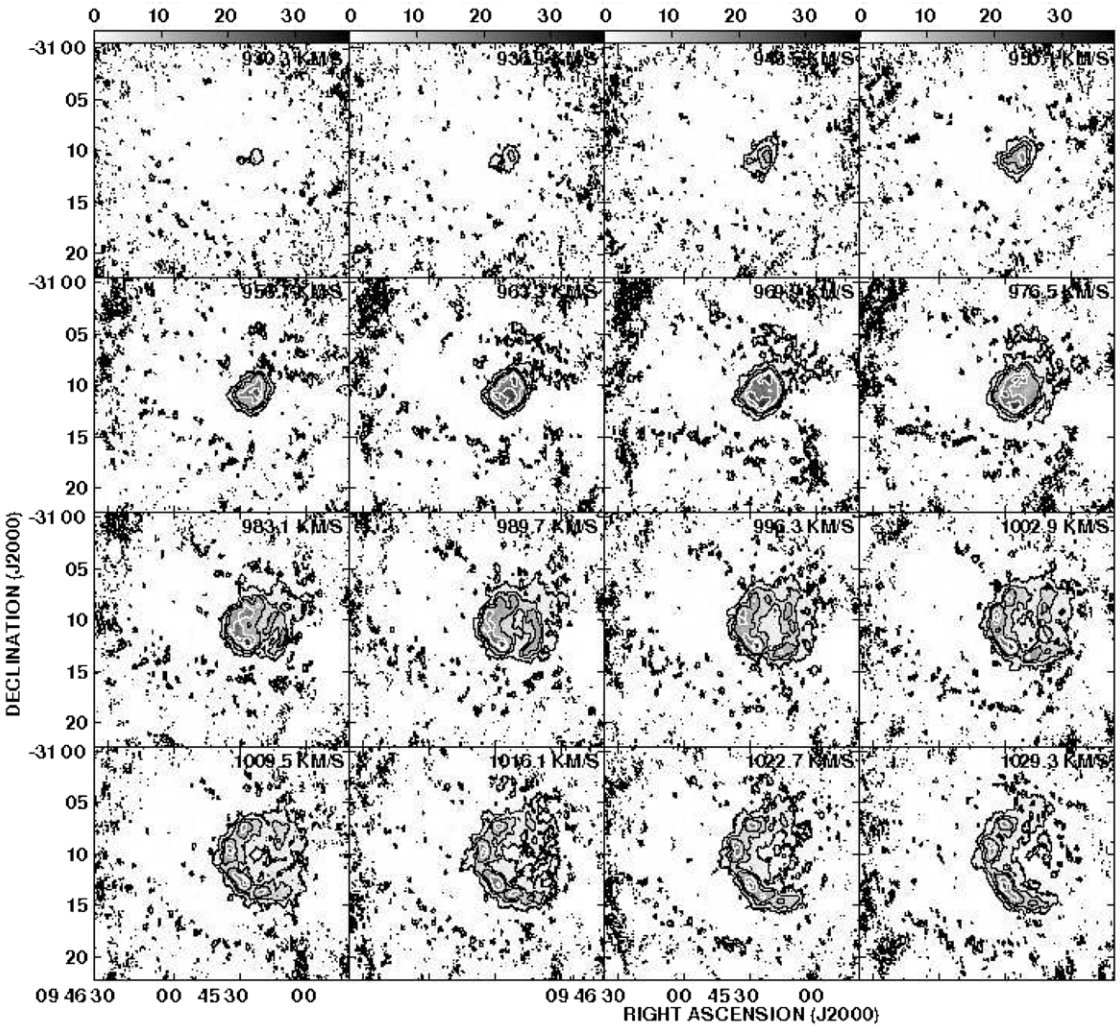

Figure 1. Channel maps of NGC 2997 covering 930.3 to 1029.3 km s^{-1} heliocentric velocity. Data are plotted at full spatial and spectral resolution. Contours are plotted for 3σ, 10σ, 20σ, 40σ, and 60σ, where $\sigma = 1.9 \times 10^{19}$ cm^{-2} beam^{-1} channel^{-1}. Gray scale is in units of mJy beam^{-1}.

We trust this rotation curve to ∼28 kpc, beyond which the lopsidedness of the H I emission produces large errors in the fit. In addition, in order to understand the quality of our assumption that the disk is flat and ideal, we refit the rotation curve allowing the inclination and the position angle to vary while keeping the rotational velocity fixed to the value found for each ring in the tilted ring model. The middle and bottom panels of Figure 7 show how the inclination and position angle, respectively, vary with radius. In these instances the rotational velocity for each ring is fixed to the value plotted in the top panel.

There is evidence that NGC 2997 deviates from the ideal, flat disk. The bottom panel of Figure 7 suggests that we were unable to fit a self-consistent rotation curve with a uniform position angle because it declines steadily with radius. In the tilted-ring model, inclination and rotation velocity are coupled through a $v_{\rm rot} \sin i$ term. This makes for a degeneracy between a flat inclination and falling rotation curve that is particularly strong for low-inclination galaxies. The "S" like appearance of contours near the minor axis (Figure 4) indicate that NGC 2997 may have a slightly warped H I disk.

3.2. Modeling the Lagging Thick Disk

Our deep observations of NGC 2997 show that the H I gas is not confined to the thin disk. In PV slices the contours of H I emission show a shallow gradient toward the systemic velocity: a feature which has been identified in a small number of other galaxies and has been referred to as a "beard" (e.g., NGC 2403; Schaap et al. 2000; Fraternali et al. 2002). After modeling the dominant H I component, we subtract the thin disk from the original data cube and find that 1.4×10^9 $M_\odot$ of residual H I emission remains—about 18% of the total $M_{\rm H\,I}$ of the galaxy.

This second component can be fit by a Gaussian with a higher velocity dispersion than the thin disk (∼ 16 km s^{-1}) which reflects the thermal motions of the gas convolved with a vertical velocity gradient (de Blok & Walter 2006). The peak velocity of the fitted Gaussian resides closer to the systemic velocity of the galaxy than gas in the thin disk at the same radius. In other words, it appears to follow galactic rotation, but at slower rotational velocities. We fit a second rotation curve to the residual data by assuming that this thick disk has the same large-scale morphology as the thin disk, with the same systemic velocity (1089 km s^{-1}), position angle (107°) and inclination (32°). From Figure 8 we see that peaks in the two rotation curves roughly coincide with one another, implying that they are related, however the thick disk consistently lags behind that of the thin disk by ∼60 km s^{-1}. A similar lagging disk has been observed in NGC 891 (25–200 km s^{-1}; Swaters et al. 1997) and NGC 2403 (25–50 km s^{-1}; Schaap et al. 2000; Fraternali et al. 2002).

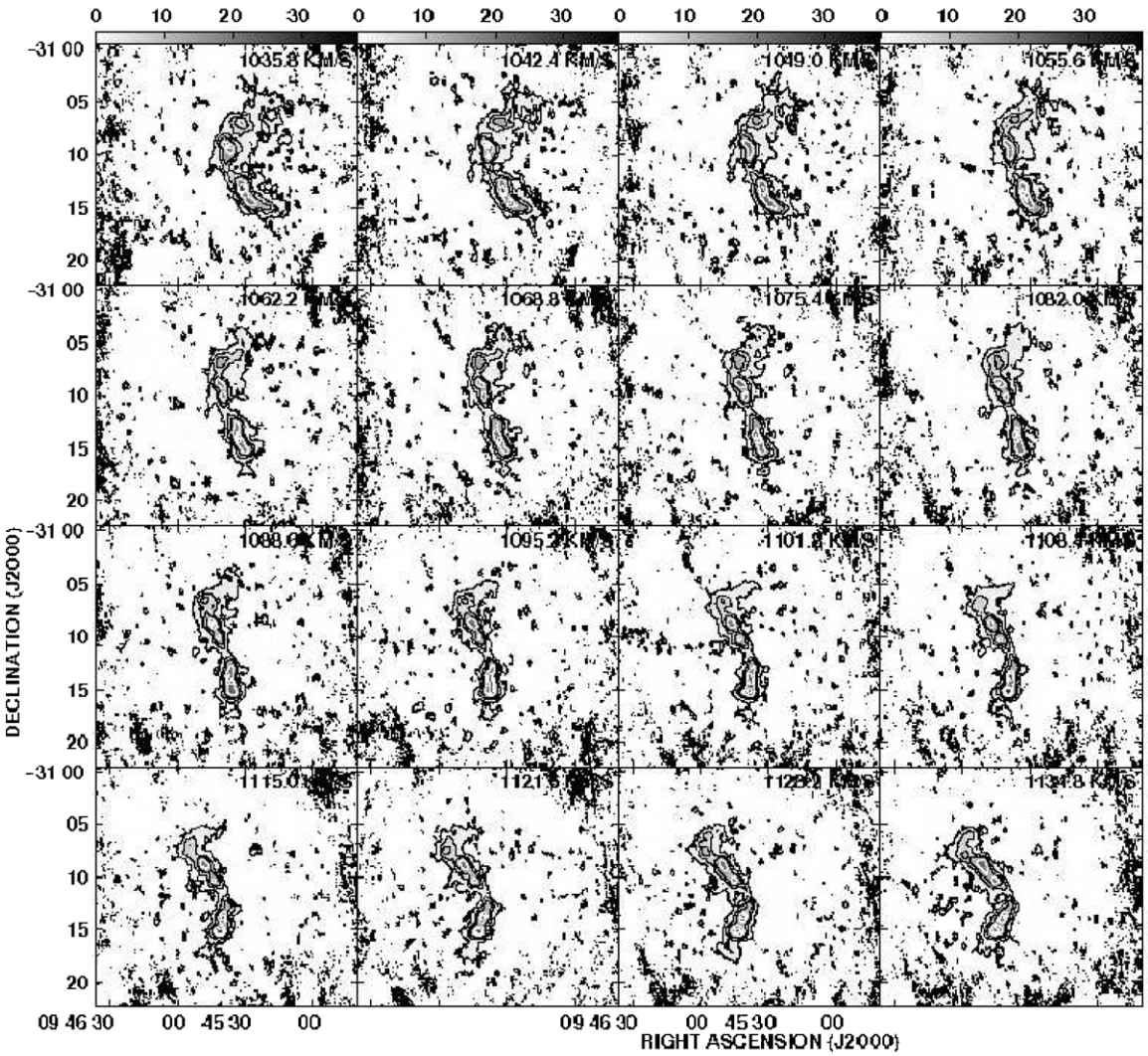

Figure 2. As in Figure 1 but covering 1035.8 to 1134.8 km s^{-1}.

To understand this relation we also attempted to derive the thick disk rotation curve from the residual data without assuming it has the same properties as the thin disk. While we successfully fit a position angle ($\sim$25°), we were unable to find a consistent inclination. In NGC 2403, Fraternali et al. (2002) show that a rotated position angle, such as this can be explained by an overall inflow of the anomalous gas. However, as we find no other evidence for radial gas motion when we include it in our models of NGC 2997, we disregard it.

We took this kinematic modeling a step further by adding a velocity gradient to the rotation curve as a function of height above the disk midplane. We followed similar procedures to those demonstrated by Heald et al. (2006b) and Oosterloo et al. (2007). The GIPSY task GALMOD allows one to create a model data cube from user supplied parameters: the rotational velocity, the scale height and the surface density. A modified version of this task (G. H. Heald 2008, private communication) includes two additional parameters to specify (1) the rate of change in velocity, dv/dz, with height, z, and (2) a cylindrical height above the disk at which the gradient begins, $z_{\rm cyl}$, such that the rotation of the gas is described by the following equations:

$$v_{\rm rot}(R,z) = \begin{cases} v_{\rm rot}(R,0) & z \leqslant z_{\rm cyl}, \\ v_{\rm rot}(R,0) - (z - z_{\rm cyl})\frac{dv}{dz} & z \geqslant z_{\rm cyl} \end{cases}. \quad (1)$$

We examined PV slices along the galaxy's major axis to compare the models created from the modified GALMOD task with our data (Figure 9).

The cylindrical height was the easiest parameter to fit. It is defined as the distance from the midplane at which the velocity gradient begins. Setting its value has the effect of imposing the velocity at which the peak of the emission occurs. For example, with a smaller cylindrical height the velocity gradient begins closer to the midplane and, for an inclined galaxy, the resulting sum of emission projected along the line of sight appears to shift toward lower velocities. A cylindrical height of 0.5 ± 0.1 kpc fits our data best. This is within the range of values derived for other galaxies: Heald et al. (2007) report values ranging from 0.4 kpc in NGC 4302 to 1.2 kpc in NGC 5775 using Hα kinematics of ionized gas; while Oosterloo et al. (2007) report a value of 1.3 kpc for NGC 891 in H I.

The value of the scale height predominately influences the lowest level H I contours of the PV diagram. A large-scale height places more emitting material at greater distances from the disk and, therefore, at lower velocities with respect to the rotational velocity at the midplane so the H I contours become shallower toward the systemic velocity with increasing scale height. The best fit for the scale height is 0.7 ± 0.2 kpc. Our errors are based on the resolution of parameter space sampled

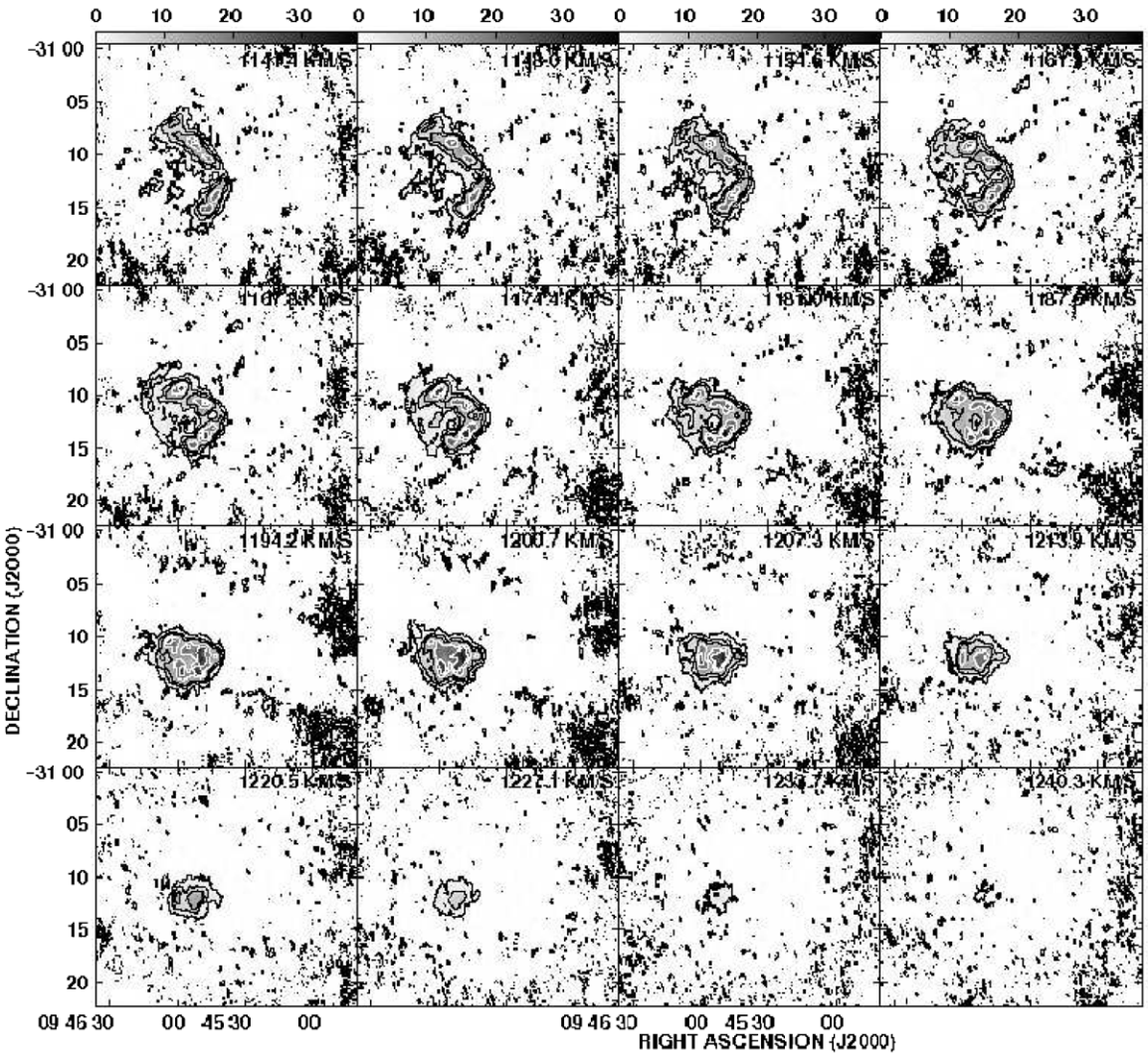

Figure 3. As in Figure 1 but covering 1141.3 to 1240.3 km s^{-1}.

and the degree to which the models differed significantly by eye.

The model is least sensitive to the velocity gradient, probably due to NGC 2997's relatively low-inclination and the low-column density of the gas in the lagging disk. Varying this value changes the gradient of the H I contours in the model, however it does so less dramatically than varying the scale height. This, combined with the clumpiness of the H I due to spiral arms and other features in the disk, makes it difficult to estimate a good fit. We estimate the velocity gradient to be between 18–31 km s^{-1} kpc^{-1}. Again, these values fall in the range reported for NGC 4302 (22.8–59.2 km s^{-1} kpc^{-1}; Heald et al. 2007), NGC 5775 (8 km s^{-1} kpc^{-1}; Heald et al. 2006b), and NGC 891 (15 km s^{-1} kpc^{-1}; Oosterloo et al. 2007).

3.3. Anomalous H I

In spite of this extensive modeling, there is a significant amount of remaining H I that is spatially or kinematically distinct from the disk gas. In order to identify this faint emission we Hanning smoothed in velocity and spatially smoothed the data to twice the original beam size. The resulting cube has a resolution of $28'' \times 22''$. The rms noise improves to $\sigma = 0.15$ mJy beam^{-1}, or a 5σ mass sensitivity of $1.7 \times 10^5\ M_\odot$ channel^{-1} and column density of 8.9×10^{18} cm^{-2} beam^{-1} channel^{-1}. We visually searched this cube and found several examples of anomalous H I features whose basic properties are presented in Table 3: their projected radial distance from the center of the galaxy, their velocity offset from the H I disk, and their H I mass as well as an estimate for their contribution to the mass accretion rate. This is not an exhaustive list, but merely illustrates some of the most prominent examples of HVC analogs associated with NGC 2997. Figure 10 shows where we have taken slices through the smoothed data cube to present these features in Figures 11(a)–(d).

Of these anomalous features, we find five examples of H I clouds that are completely distinct from the H I disk. They were identified in PV slices as having velocity offsets of greater than 50 km s^{-1} from H I gas in the disk at the same position (Figures 10 and 11). In three of the five examples, the H I gas is counter-rotating with respect to the H I disk (slices (a) and (c)), and in one instance we find an H I cloud whose velocity component along the line of sight is actually faster than the rotation of the disk (slice (b)). The clouds we identify reside within 20 kpc from the center of the galaxy, which places them within the extent of the projected H I disk, but outside the optical disk as it is seen in DSS images (Figure 4), and they all have H I masses of approximately $10^7\ M_\odot$. They were not detected by Pisano et al. (2007) because of the low angular

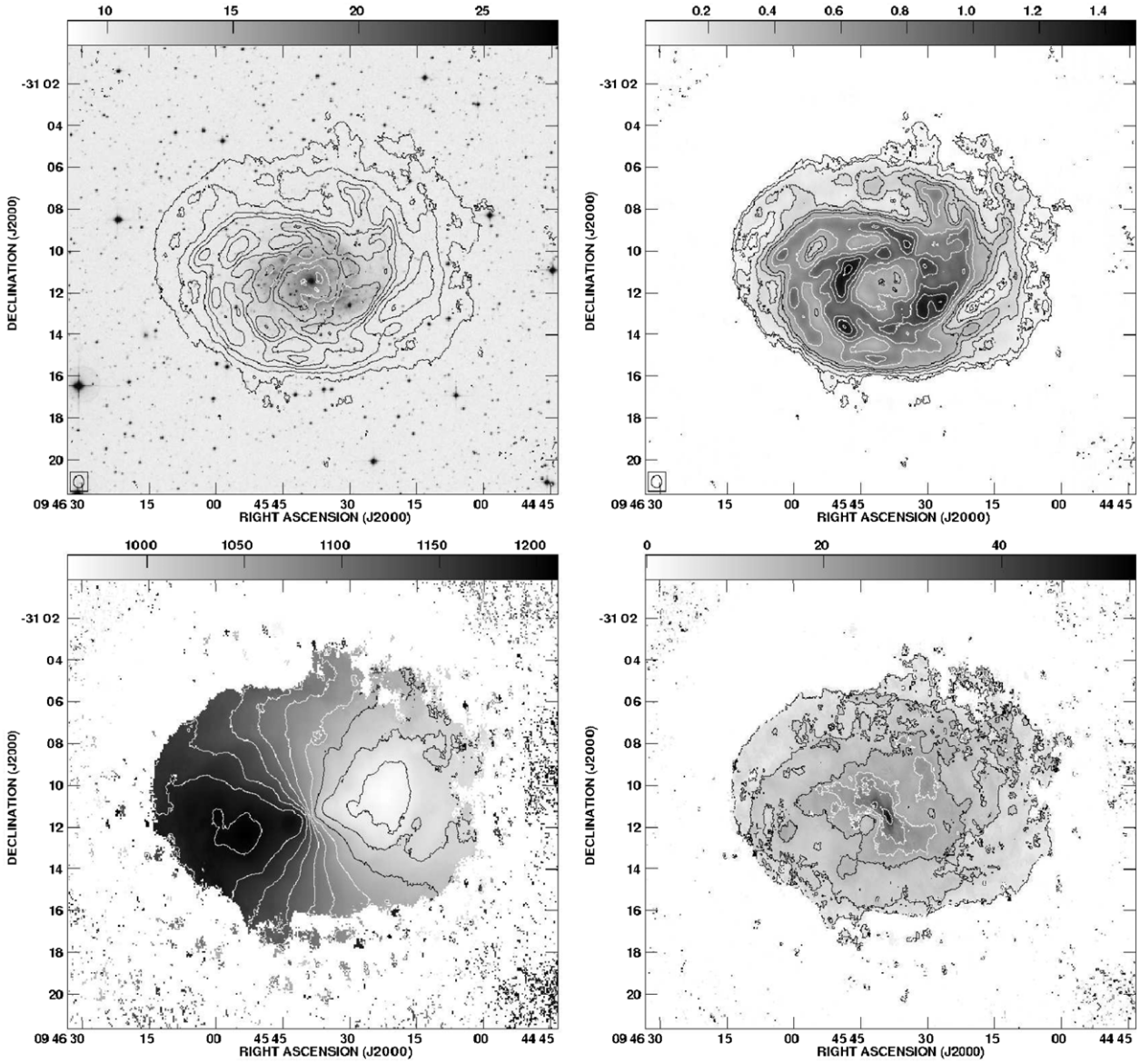

Figure 4. Top left: DSS image of NGC 2997 overlaid with H I contours. Top right: H I total intensity map; contours are at 5σ, 20σ, 50σ, 80σ, 120σ, where $\sigma = 1.9 \times 10^{19}$ cm^{-2} beam^{-1} channel^{-1}. Gray scale is in units of Jy beam^{-1}. Bottom left: intensity weighted velocity map of NGC 2997; contours range over 975–1200 km s^{-1} and are spaced every 25 km s^{-1}. Bottom right: the intensity weighted velocity dispersion map; contours are at 4, 10, 15, 20, 25, and 40 km s^{-1}.

resolution of their Parkes (14′) and ATCA ($\sim$ 1′) data. There are significant indications of a larger population of H I clouds around NGC 2997, however we are less confident in their identification because they are closer to our mass sensitivity limit and because of residual phase calibration errors in the data cube.

In addition to the H I clouds, there are two other prominent features of anomalous H I we see in velocity channels: a "spur" of counter-rotating gas near the center of the galaxy and a "tail" of emission lagging in rotation, extending to the west from the north half of the galaxy. Unlike the H I clouds which are distinct, both of these features are connected to the main disk of the galaxy (making it difficult to estimate their mass). The "spur" is attached north of the center, and arcs to the east and south extending greater than 6 kpc east from the center of the galaxy (v = 1016.1–1082.0 km s^{-1} in Figures 1 and 2). In PV slices the same feature looks like a shell of emission that is connected to the disk (Figures 11(b)–(d)). We estimate the H I mass in the spur to be $\sim 2.6 \times 10^7$ $M_\odot$. The "tail" contributes to the asymmetry total intensity map (Figure 4). Although the contours of the intensity weighted velocity map (Figure 4) are well behaved, individual velocity channels, v = 943.5–983.1 km s^{-1} (Figure 1), show emission on the north side of the galaxy. The coherence of this emission can be seen in slices (a) and (b) of Figure 11: the feature looks like a bifurcation of the H I disk in PV space. Its velocity component along the line of sight is actually moving faster than the rotation of the disk. We calculate the mass of the tail to be 3.1×10^7 $M_\odot$.

4. DISCUSSION

In addition to the thin disk of NGC 2997, seen in most spiral galaxies, we have identified two additional H I components that are not as ubiquitous: a lagging, thick disk, and anomalous H I clouds. The thick disk has a mass of 1.4×10^9 $M_\odot$, a broader velocity dispersion, $\sim$16 km s^{-1}, and lags behind the rotational velocity of the thin disk by $\sim$ 60 km s^{-1}. The anomalous H I clouds are spatially or kinematically distinct from both H I disk components. The clouds have individual H I masses between $10^{6.7}$–$10^{7.3}$ $M_\odot$, are offset from the disk by 80–200 km s^{-1}

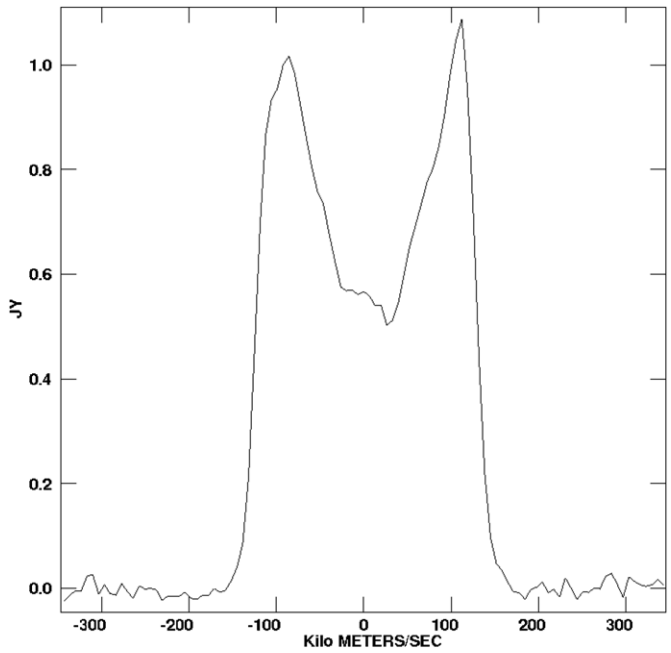

Figure 5. Integrated H I profile of NGC 2997 over the full H I extent of the galaxy. The profile is centered on the systemic velocity of the galaxy, 1089 km s^{-1}.

and, in some instances, are counter-rotating. In this section, we compare our results with the distribution of H I observed around other galaxies, we speculate on the possible origins of NGC 2297's HVC analogs, we discuss our results in the context of the Local Group HVCs, and we examine the effect of our distance estimate on our conclusions.

4.1. Extraplanar H I

NGC 2997 is one of the lowest inclination galaxies in which a lagging disk has been modeled. It is impossible to do this same decomposition for a face-on galaxy because the measured velocities contain no information on the rotation of the gas, but moderate to high-inclination galaxies are well suited to this analysis. The velocity gradient we estimate for NGC 2997, 18–31 km s^{-1} kpc^{-1}, appears to be typical of spiral galaxies for which deep observations reveal extended extraplanar gas. Our findings are consistent with that seen in NGC 2403 where Fraternali et al. (2001) calculate the thick disk to have a mean rotation velocity 25–50 km s^{-1} lower than that of the thin disk, in NGC 4459 where Barbieri et al. (2005) find a thick disk that lags by 12–25 km s^{-1}, and in NGC 891, where the velocity gradient ranges from 14 to 43 km s^{-1} kpc^{-1} depending on the location in the galaxy (Oosterloo et al. 2007). NGC 6946 also has a similar lagging halo of cold gas (Boomsma et al. 2009).

This range of values for the velocity gradient in spiral galaxies suggests that one might correlate it with star formation activity. Heald et al. (2006a, 2006b, 2007) have done a complementary study of three high-inclination galaxies, NGC 5775, NGC 891, and NGC 4302, in which they find that the magnitude of the velocity gradient, measured in ionized gas (Hα), decreases with star formation activity, as measured in far-infrared luminosity. For NGC 2997, we calculate a star formation rate of 5 ± 1 $M_{\odot}$ yr^{-1} from 60 and 100 μm IRAS fluxes (following Kewley et al. 2002; Bell 2003) and 1.4 GHz fluxes (following Condon et al. 2002; Bell 2003). However, it is unclear how well NGC 2997 supports such a correlation: its values for the velocity gradient and scale height are close to the mean of those galaxies, while the star formation rate is a bit high. Heald et al. (2007) also suggest that the product of the velocity gradient and the scale height tends toward 20 km s^{-1}. We estimate $dv/dh_z = 12$ –21 km s^{-1}, which is consistent with their suggestion.

From a theoretical standpoint, the detection of a thick, lagging disk is consistent with the idea developed by Bregman (1980) in which the Galactic HVCs are clouds condensing out of a hot Galactic corona fed by SNe in the disk. In his galactic fountain model, gas blown out of the disk by star formation moves radially outward and slows down to conserve angular

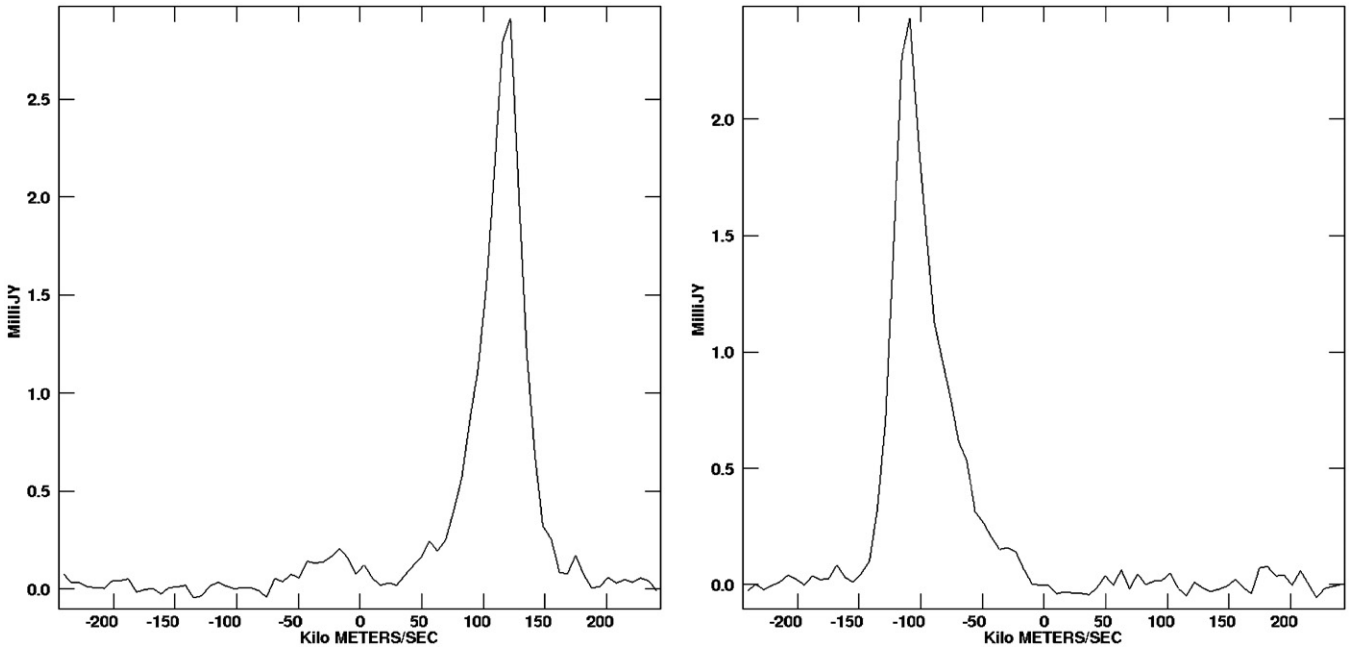

Figure 6. Left: a sample spectrum toward a position on the eastern side of NGC 2997 showing the thin disk rotation at ∼120 km s^{-1}; the asymmetry of the H I profile, characteristic of the thick disk, at ∼60 km s^{-1}; and anomalous H I at ∼ −25 km s^{-1}. Right: a spectrum from the western side of the galaxy illustrating the thin (∼110 km s^{-1}) and thick disk (∼50 km s^{-1}) components. The spectra are centered on the systemic velocity of the galaxy, 1089 km s^{-1}.

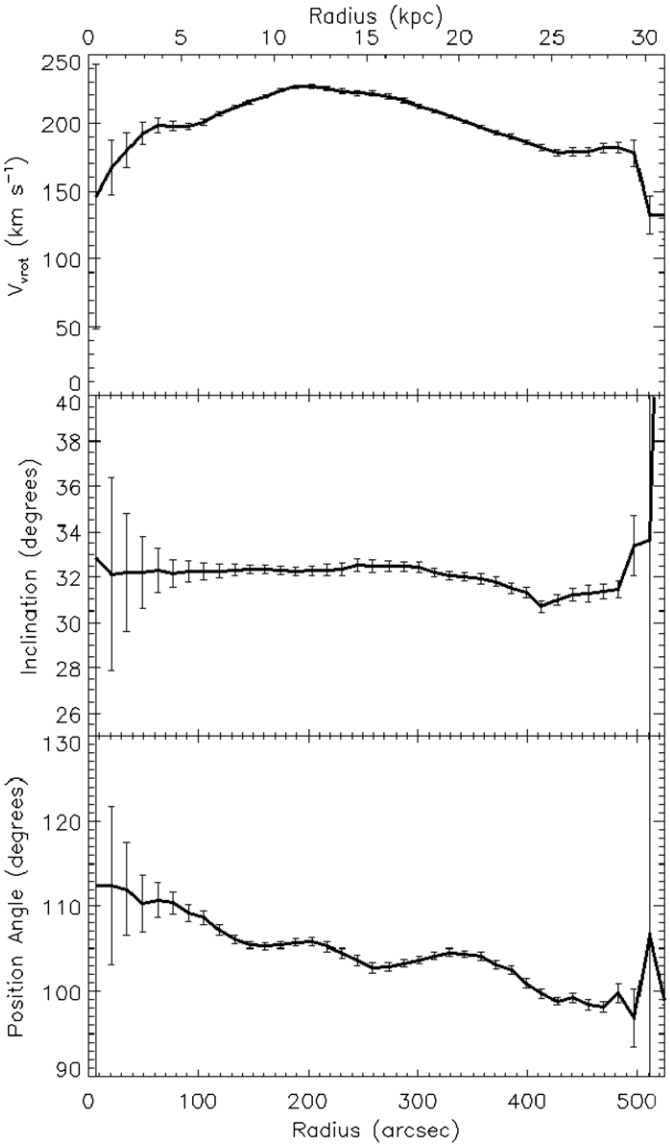

Figure 7. Top panel is our rotation curve derived from a tilted ring model. It peaks at 226 km s^{-1} around 12 kpc. The two bottom panels demonstrate the quality of our assumption that NGC 2997 is an ideal, flat disk. We keep all other parameters fixed but allow the inclination (middle) and position angle (bottom) to vary—the rotational velocity for each tilted ring is fixed to the value found in the top panel. The declining position angle with radius suggests we were unable to fit a self-consistent rotation curve.

momentum as it moves vertically away from the midplane. If the observed lag is only due to conservation of angular momentum then, in the case of NGC 2997, gas that lags by 60 km s^{-1} behind a disk rotating at 200 km s^{-1} originated 70% closer to the center of the galaxy. However, if hydrodynamic effects are important, the radial motion is less dramatic. Cooling gas condenses out of the corona and moves inward again. Evidence for radial inflow of 10–20 km s^{-1} has been observed in NGC 2403 (Fraternali et al. 2001) and perhaps in NGC 4559 (Barbieri et al. 2005). We do not find evidence for radial inflow of H I in NGC 2997, but such a signature may be ambiguous due to the low inclination of the galaxy. Radially infalling clouds would also be expected if these clouds originated in a cooling hot galactic halo that is at the virial temperature of the dark matter halo as proposed by Maller & Bullock (2004), however holes in the H I disk may be evidence that SNe are responsible for circulating this gas.

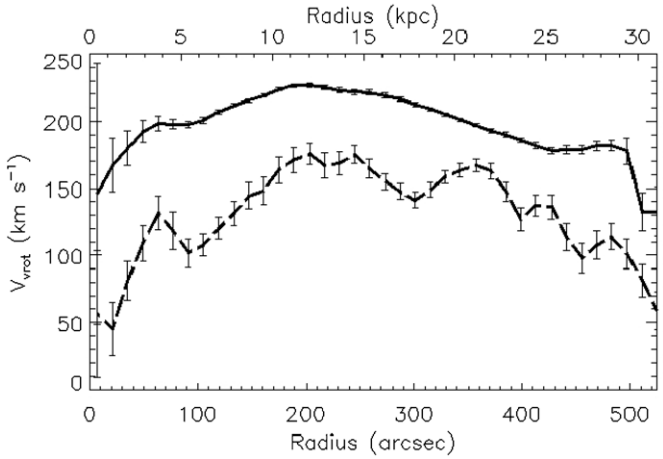

Figure 8. Rotation curves for both the thin disk (solid line) and the thick disk (dashed line). The average Δv between the rotation curves is about 60 km s^{-1}.

In a number of cases where we see anomalous H I clouds in PV slices, we also see depressions in the H I column density in the disk (slices (b) and (d)). These H I "holes" occur near the outskirts of the H I disk, but outside of the optical disk, and we hesitate at calling them holes because they frequently occur between two H I spiral arms. These may be sites where H I has been blown out of the disk from SNe, however one cannot rule out that these may also be the result of a dwarf galaxy that has impacted the disk. For example, this may be the case for large holes in NGC 6946 (Boomsma et al. 2009) and M 101 (van der Hulst & Sancisi 1988). In any case, it is interesting to note that all of the anomalous H I we identify is coincident with the H I disk and we do not find any large H I clouds far from it.

The large clouds of counter-rotating H I gas and the "spur" cannot be explained by a galactic fountain mechanism. While fountain gas lags behind the main disk in rotation, it will conserve angular momentum and so can not be counter-rotating. Additionally, to eject clouds of 10^7 $M_\odot$ from the disk at the observed velocity offsets requires an spatially and temporally coherent injection of 10^{54} erg of energy. This corresponds to of order 10^4 SNe, assuming 10% efficiency. Despite the star formation rate of NGC 2997, this appears to be implausibly high. Based on this energy argument, and their position with respect to the optical disk, we conclude that these H I features are more likely material being accreted by NGC 2997, either out of a hot galactic halo (Peek et al. 2008), or are the remnants of a tidally disrupted gas rich dwarf galaxy. The maximum individual cloud mass from the Peek et al. (2008) simulations is 5×10^6 $M_\odot$, however they do not rule out the possibility of cloud complexes having higher masses. We estimate a lower limit for the total accretion rate of 1.2 $M_\odot$ yr^{-1}, which may help sustain the vigorous star formation rate, especially if it is augmented by gas from the lagging disk which one would expect to eventually fall back toward the midplane.

Features such as the asymmetry in the extended northwest spiral arm are usually interpreted as evidence for past interactions between galaxies, and there are two possible culprits. The nearest LGG 180 group galaxy is a dwarf galaxy, ESO 434-G041, which is ∼115 kpc to the southeast. It is resolved in our ATCA observations, but lies outside the primary beam of the GMRT. NASA/IPAC Extragalactic Database (NED) lists another dwarf galaxy, ESO 434-G030, ∼90 kpc to the southwest, but we do not see this galaxy in our data. Assuming that the velocity

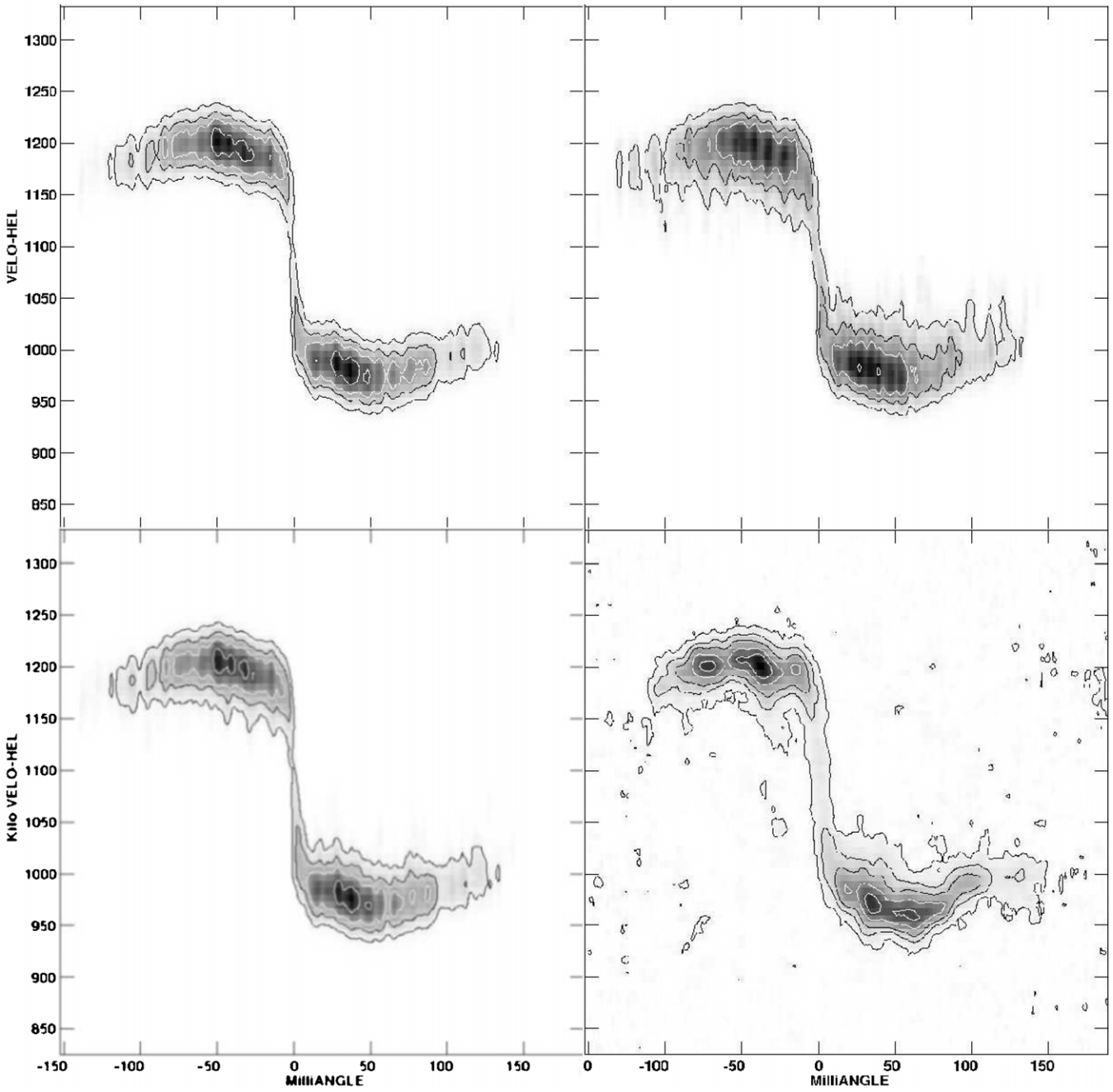

Figure 9. Limiting examples of our lagging disk models. Upper left: the best scale height and z_{cyl}, but too small a velocity gradient: there is not enough emission close to the systemic velocity. Upper right: the best velocity gradient and z_{cyl}, but no scale height: the emission is more spread out in velocity space, and the peak is lower in intensity and closer to the systemic velocity than seen in the data. Lower left: our best-fit model with scale height = 0.8 kpc, z_{cyl} = 0.6 kpc, and velocity gradient = 38 km s^{-1} kpc^{-1}. Lower right: the data. Contours are at 3σ, 10σ, 20σ, 40σ, and 60σ, where $\sigma = 1.9 \times 10^{19}$ cm^{-2} beam^{-1} channel^{-1}.

differences in the plane of the sky are similar to the line-of-sight velocity differences between these galaxies and NGC 2997, any encounter would have taken place ∼1 Gyr ago. While there are no apparent connections between these galaxies and NGC 2997 in H I, nor any optical signatures of disturbances in the dwarf galaxies, a past tidal event or interaction seems to be the most likely explanation for pulling such a large amount of H I from the disk in such a coherent manner, causing the asymmetry. On the other hand, we do not believe that interactions are the most probable origin for the anomalous H I clouds. Similarly, the "tail" feature, on the northwest side of the galaxy, seems best explained by accretion—perhaps a dwarf galaxy that has been tidally disrupted as it passed near NGC 2997.

4.2. Comparison with M 31 Clouds and Galactic HVCs

We have identified the most massive anomalous H I clouds associated with NGC 2297. These five clouds have masses of order 10^7 $M_\odot$. The spectrum of cloud masses extends to lower masses but, in many cases, it is difficult to separate them as distinct from emission in the thick disk. Nonetheless, we can still compare the clouds we have identified with those reported in the Local Group and around other galaxies.

The H I mass distribution of clouds in M 31 given by $dM(M_{HI}) \propto {M_{HI}}^{-2} dM_{HI}$, allows us to estimate the total number of similar clouds we should expect to see around NGC 2997. Most clouds have masses in the range $(0.15–1.3) \times 10^6 M_\odot$ with only Davies'

Table 3
Properties of Anomalous H I Clouds in NGC 2997

Obj. ID	Distance (kpc)	Velocity[a] (km s^{-1})	TF Mass[b] ($M_\odot$)	Accretion Rate[c] ($M_\odot$ yr^{-1})	Notes
Cloud 1	17.7	120	$1.9 \pm 0.2 \times 10^7$	0.13	Figure 11(a)
Cloud 2	13.0	−105	$7.6 \pm 0.1 \times 10^6$	0.06	Figure 11(b)
Cloud 3	18.9	150	$8.6 \pm 0.4 \times 10^6$	0.07	Figure 11(c)
Cloud 4	14.2	80	$8.9 \pm 0.8 \times 10^6$	0.05	Figure 11(d)
Cloud 5	10.4	200	$4.9 \pm 0.4 \times 10^6$	0.10	Figure 11(a)
H I Spur	5.9	150	$2.6 \pm 0.1 \times 10^7$	0.70	Figures 11(b)–(d)
H I Tail	27.8	−60	$3.1 \pm 0.3 \times 10^7$	0.07	Figures 11(a) and (b)

Notes.
[a] Negative indicates a line-of-sight velocity faster than the rotational velocity of the disk at that position.
[b] The accretion rate is estimated from $M_{\rm H\,I\,cloud} \times v_{\rm offset}/r$ where $v_{\rm offset}$ is the velocity difference between the cloud and gas in the thin H I disk, and r is the projected distance of the cloud from the center of the galaxy.

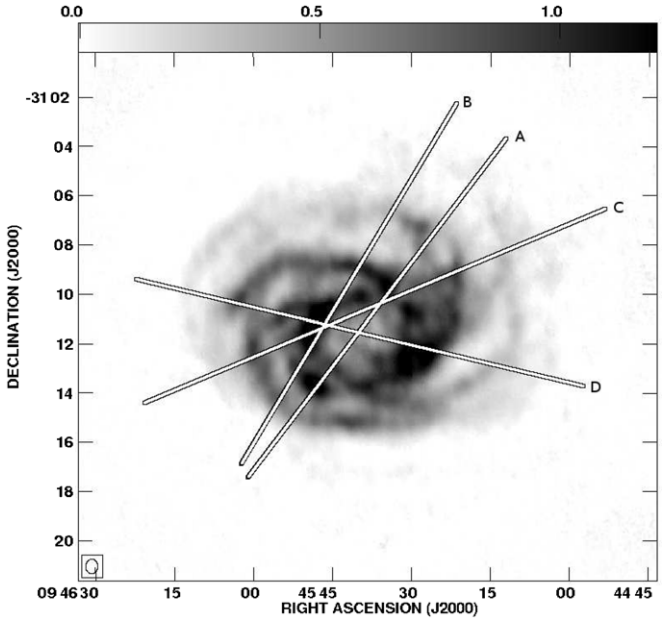

Figure 10. Total intensity H I map of NGC 2997 illustrating where slices have been made to analyze the anomalous H I content (see Figure 11).

Cloud having $M_{\rm H\,I} = 10^7\ M_\odot$. For sources seen by Thilker et al. (2004) smaller than our beamsize, we would expect to detect about 10 of the M 31 HVC analogs at the 5σ level (and about 4 above the 10σ level); for those clouds that we could resolve, we lack the column density sensitivity to detect them. However, we already know from the observations of Pisano et al. (2007) that there are no low column density H I clouds residing off the disk of NGC 2997. The HVCs discovered around M 31 in higher resolution images by Westmeier et al. (2005) have an average size of 1 kpc (equivalent to the size of our beam at the distance of NGC 2997) and are below our detection limits.

With recently determined distant brackets to Milky Way HVCs, we can put our H I clouds into a local context. For Complex C, Wakker et al. (2007) estimate $M_{\rm H\,I}$ to be (0.7–6) × $10^6\ M_\odot$. The H I masses for four other clouds range from (0.09–0.41) × $10^4\ M_\odot$ (Cloud g1) to (0.68–1.60) × $10^6\ M_\odot$ (Complex GCP; Wakker et al. 2008). Therefore, at the distance of NGC 2997, we are only sensitive to the most massive Milky Way HVCs for which distance measurements exist. However, we also see more massive features ($\sim 10^7\ M_\odot$) for which their are few counterparts around the Milky Way and M 31. Nonetheless, our discoveries are consistent with anomalous H I clouds observed in other galaxies (Sancisi et al. 2008, and references therein).

4.3. Implications of the Distance Estimate to NGC 2997

The distribution of H I clouds we find around NGC 2997 can be used to place limits on cosmological and large-scale structure simulations for the number of small dark matter halos around massive galaxies. The H I masses we calculate depend on the square of the assumed distance to the galaxy. However, local large-scale structure results in an inaccurate distance estimate to NGC 2997 because its peculiar velocity is not dominated by Hubble flow. Unfortunately, an attempt to correct for this, the velocity flow model of Masters (2005), is sparsely populated by galaxies in the volume around NGC 2997, so we choose to calculate the distance to NGC 2997 using the TF relation.

The TF relations based on near-infrared observations may be the most reliable because they are less impacted by dust than optical magnitudes. We retrieved the 2MASS *J*-, *H*-, and *K*-band magnitudes from NED and used the bias corrected TF parameters specific to Sc galaxies (Masters et al. 2008; Table 2):

$$M(J) - 5\log h = -21.017 - 9.228(\log W - 2.5)$$
$$M(H) - 5\log h = -21.847 - 9.165(\log W - 2.5)$$
$$M(K) - 5\log h = -22.039 - 10.092(\log W - 2.5).$$

To estimate the internal extinction, we interpolated between *I* and *K* bands to get values for *J* and *H* using the formulae in Courteau et al. (2007). The FWHM of the H I profile ($W = 445$ km s^{-1}) comes from Parkes observations (Pisano et al. 2007; D. J. Pisano et al. 2009, in preparation), corrected for instrumental effects, turbulent motions, cosmological broadening, and inclination as per the formula in Masters et al. (2008). From these 2MASS TF relations we derive a mean distance of 12.2 ± 0.9 Mpc.

This new distance estimate places NGC 2997 about 10% closer to the Milky Way than the estimates found on NED, corrected for peculiar velocity due to local density enhancements, and 18% closer than the velocity flow model of Masters (2005). This places somewhat tighter constraints on the fact that we do not see a large population of H I clouds outside the disk of NGC 2997. The anomalous H I clouds within the disk, for which we calculate masses, become more consistent with those observed around M 31 and more consistent with the mass estimate for Complex C in the Milky Way. Despite this closer

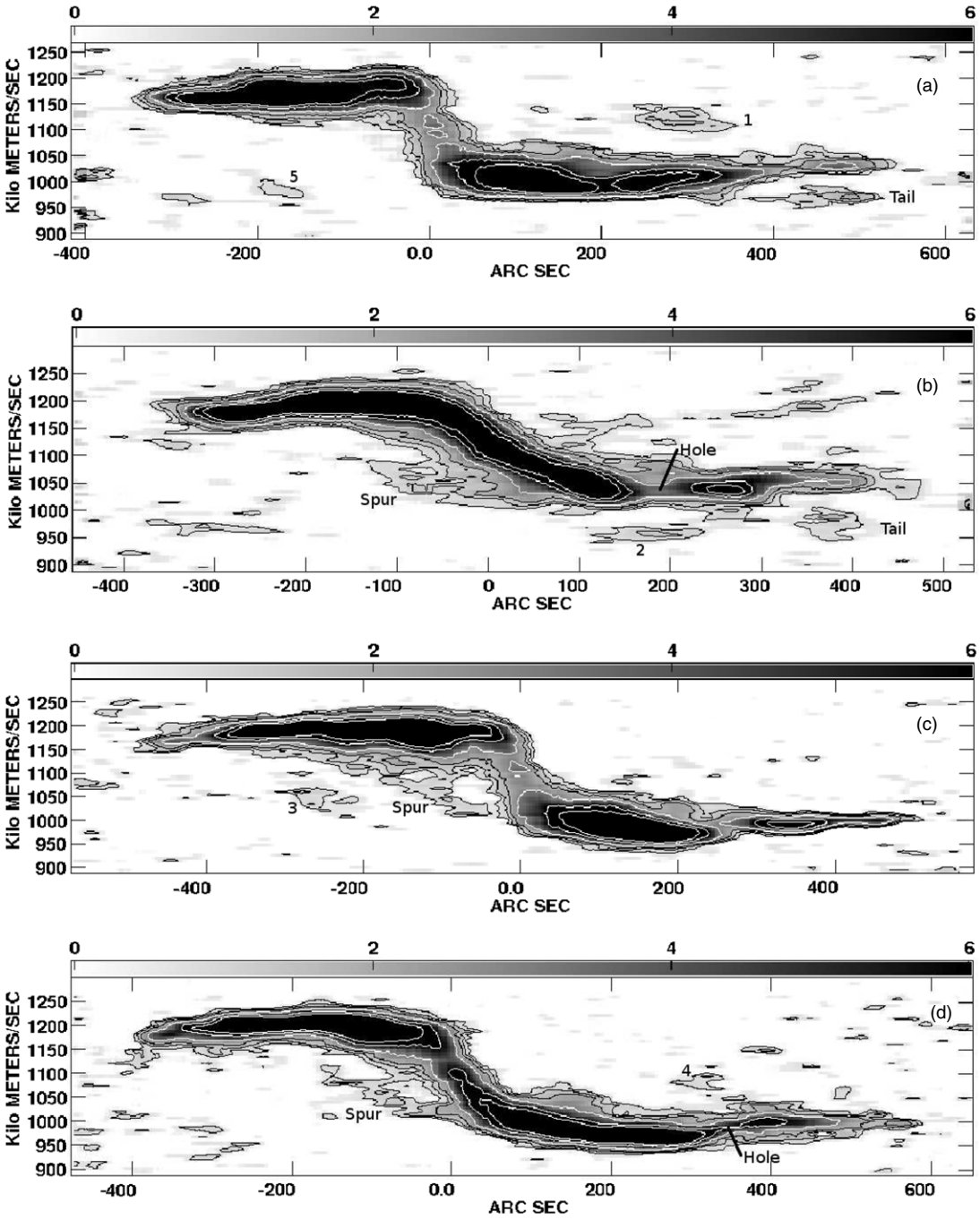

Figure 11. Select slices through the smoothed H I cube illustrate the extraplanar H I (see Figure 10 and Table 3). (a) Clouds 1, 5, and the H I tail. (b) Cloud 2 with H I hole, the H I tail, spur, and additional examples of faint, counter-rotating gas. (c) Cloud 3 and H I spur. (d) Cloud 4 with H I hole and H I spur. The positive direction corresponds to the western side of the galaxy.

distance estimate, the difference between it and previous estimates is not enough to change the formation hypotheses for the individual clouds we identify.

5. CONCLUSIONS

Our observations of NGC 2297 reveal a galaxy with lagging, thick disk and anomalous H I clouds in the halo similar to other galaxies, such as NGC 2403 (Fraternali et al. 2001) and NGC 6946 (Boomsma et al. 2009). The presence of a lagging disk, which may be caused by star formation activity, and the presence of large H I clouds and counter-rotating gas from accretion show that many processes contribute to the distribution of this cold gas.

We propose that the lagging disk is the result of a galactic fountain process in which gas is blown out of the disk by SNe. This gas experiences a decreasing gravitational force as it moves away from the midplane, so it drifts radially outward. As a result, this gas rotates in the same sense as the thin disk, but at slower velocities to conserve angular momentum. From *IRAS* 60 and 100 μm, and 1.4 GHz radio continuum fluxes we estimate fairly vigorous star formation rate in NGC 2997 of about 5 $M_{\odot}$ yr^{-1}

to support the renewal of this lagging disk. Of the total H I mass of the galaxy, 16%–17% resides in this lagging disk.

The most likely origin for the H I clouds we discover is accretion from a hot galactic halo or from nearby dark matter halos. The H I cloud masses are of order 10^7 $M_\odot$. From their velocity offset with respect to nearby disk gas, we estimate a kinetic energy for the clouds relative to the rotation of the disk of $\sim 10^{54}$ erg and conclude that it is unlikely their presence is due to SNe. Meanwhile, the spur and tail may be the remnants of tidally disrupted gas-rich dwarf galaxies. The anomalous H I we identify makes up approximately 1%–2% of the total H I mass. Finally, the asymmetry of NGC 2997 to the northwest appears best explained by a tidal interaction with another galaxy, although it is not obvious whom the culprit may be.

The features we find are not out of line with those observed in the Local Group, nor compared to other galaxies for which similar observations and modeling have been done, although the clouds of NGC 2997 tend to be more massive than the clouds for which we have distance brackets in the Milky Way, even with an improved distance from the 2MASS TF relations that place NGC 2997 12%–23% closer. In spite of NGC 2997's relative isolation, we believe that a number of dynamic processes contribute to the sum of extraplanar H I gas, including star formation, accretion, and galaxy interactions. Deeper observations of NGC 2997 as have been accomplished with NGC 891 would likely continue to reveal extended structure.

We gratefully acknowledge George Heald for sharing his modified GIPSY task to model the lagging disk. We thank the anonymous referee for his/her useful comments and constructive criticism that contributed to the improvement of this paper. Finally, we thank the staff of the ATCA and GMRT who have made these observations possible. The Australia Telescope Compact Array is part of the Australia Telescope which is funded by the Commonwealth of Australia for operation as a National Facility managed by CSIRO. GMRT is run by the National Centre for Radio Astrophysics of the Tata Institute of Fundamental Research. This work was supported by the National Science Foundation through grant AST 0708002.

REFERENCES

Barbieri, C. V., Fraternali, F., Oosterloo, T., Bertin, G., Boomsma, R., & Sancisi, R. 2005, A&A, 439, 947
Begeman, K. G. 1989, A&A, 223, 47
Bell, E. F. 2003, ApJ, 586, 794
Blitz, L., Spergel, D. N., Teuben, P. J., Hartmann, D., & Burton, W. B. 1999, ApJ, 514, 818
Boomsma, R., Oosterloo, T. A., Fraternali, F., van der Hulst, J. M., & Sancisi, R. 2005, A&A, 431, 65
Boomsma, R., Oosterloo, T. A., Fraternali, F., van der Hulst, J. M., & Sancisi, R. 2009, A&A, in press (arXiv:0807.3339)
Braun, R., & Burton, W. B. 1999, A&A, 341, 437
Bregman, J. N. 1980, ApJ, 236, 577
Condon, J. J., Cotton, W. D., & Broderick, J. J. 2002, AJ, 124, 675
Courteau, S., Dutton, A. A., van den Bosch, F. C., MacArthur, L. A., Dekel, A., McIntosh, D. H., & Dale, D. A. 2007, ApJ, 671, 203
de Blok, W. J. G., & Walter, F. 2006, AJ, 131, 363
Fraternali, F., Oosterloo, T., Sancisi, R., & van Moorsel, G. 2001, ApJ, 562, L47
Fraternali, F., van Moorsel, G., Sancisi, R., & Oosterloo, T. 2002, AJ, 123, 3124
Fukugita, M., & Peebles, P. J. E. 2006, ApJ, 639, 590
Garcia, A. M. 1993, VizieR Online Data Catalog, 410, 47
Heald, G. H., Rand, R. J., Benjamin, R. A., & Bershady, M. A. 2006a, ApJ, 647, 1018
Heald, G. H., Rand, R. J., Benjamin, R. A., & Bershady, M. A. 2007, ApJ, 663, 933
Heald, G. H., Rand, R. J., Benjamin, R. A., Collins, J. A., & Bland-Hawthorn, J. 2006b, ApJ, 636, 181
Kamphuis, J., & Briggs, F. 1992, A&A, 253, 335
Kamphuis, J., & Sancisi, R. 1993, A&A, 273, L31
Kewley, L. J., Geller, M. J., Jansen, R. A., & Dopita, M. A. 2002, AJ, 124, 3135
Klypin, A., Kravtsov, A. V., Valenzuela, O., & Prada, F. 1999, ApJ, 522, 82
Lockman, F. J. 2003, ApJ, 591, L33
Lockman, F. J., Benjamin, R. A., Heroux, A. J., & Langston, G. I. 2008, ApJ, 679, L21
Maller, A. H., & Bullock, J. S. 2004, MNRAS, 355, 694
Masters, K. L. 2005, PhD thesis, Cornell Univ.
Masters, K. L., Springob, C. M., & Huchra, J. P. 2008, AJ, 135, 1738
McClure-Griffiths, N. M., et al. 2008, ApJ, 673, L143
Meyer, M. J., et al. 2004, MNRAS, 350, 1195
Muller, C. A., Oort, J. H., & Raimond, E. 1963, Acad. Sci. Paris, 257, 1661
Oort, J. H. 1970, A&A, 7, 381
Oosterloo, T., Fraternali, F., & Sancisi, R. 2007, AJ, 134, 1019
Peek, J. E. G., Putman, M. E., & Sommer-Larsen, J. 2008, ApJ, 674, 227
Pisano, D. J., Barnes, D. G., Gibson, B. K., Staveley-Smith, L., Freeman, K. C., & Kilborn, V. A. 2007, ApJ, 662, 959
Putman, M. E., Thom, C., Gibson, B. K., & Staveley-Smith, L. 2004, ApJ, 603, L77
Sancisi, R., Fraternali, F., Oosterloo, T., & van der Hulst, T. 2008, A&AR, 15, 189
Sault, R., & Killeen, N. 2008, Miriad User Guide
Schaap, W. E., Sancisi, R., & Swaters, R. A. 2000, A&A, 356, L49
Shapiro, P. R., & Field, G. B. 1976, ApJ, 205, 762
Sommer-Larsen, J. 2006, ApJ, 644, L1
Swaters, R. A., Sancisi, R., & van der Hulst, J. M. 1997, ApJ, 491, 140
Thilker, D. A., Braun, R., Walterbos, R. A. M., Corbelli, E., Lockman, F. J., Murphy, E., & Maddalena, R. 2004, ApJ, 601, L39
Thom, C., Peek, J. E. G., Putman, M. E., Heiles, C., Peek, K. M. G., & Wilhelm, R. 2007, ApJ, submitted (arXiv:0712.0612)
Thom, C., Putman, M. E., Gibson, B. K., Christlieb, N., Flynn, C., Beers, T. C., Wilhelm, R., & Lee, Y. S. 2006, ApJ, 638, L97
van der Hulst, T., & Sancisi, R. 1988, AJ, 95, 1354
Wakker, B. P., & van Woerden, H. 1997, ARA&A, 35, 217
Wakker, B. P., York, D. G., Wilhelm, R., Barentine, J. C., Richter, P., Beers, T. C., Ivezić, Ž., & Howk, J. C. 2008, ApJ, 672, 298
Wakker, B. P., et al. 2007, ApJ, 670, L113
Westmeier, T., Braun, R., & Thilker, D. 2005, A&A, 436, 101